Soft Matter

Cite this: *Soft Matter*, 2011, **7**, 10085

www.rsc.org/softmatter

PAPER

Comparative assembly of colloidal quantum dots on surface templates patterned by plasma lithography

Yongliang Yang,[a] Justin Volmering,[a] Michael Junkin[a] and Pak Kin Wong*[ab]

Received 17th June 2011, Accepted 16th August 2011
DOI: 10.1039/c1sm06142a

Plasma lithography is a template-guided self-assembly nanomanufacturing strategy for creating functional engineering devices using nanoscale and molecular building blocks. To elucidate the plasma lithography manufacturing process, the comparative binding of colloidal quantum dots on plasma patterned surface templates is investigated. In particular, fluorescence microscopy and scanning electron microscopy were performed to characterize the pH-dependent assembly of quantum dots at equilibrium conditions. Remarkably, the amino-modified quantum dots adhere favorably to plasma treated, hydrophilic areas at low pH and to untreated, hydrophobic areas at high pH. The crossover pH for this transition occurs at approximately pH 9. Similar transitions can also be observed in other molecules, including bovine serum albumin, fluorescein isothiocyanate, and poly-L-lysine. Examining the crossover pH values for different building blocks reveals that the assembly process is a result of the competition between electrostatic and van der Waals interactions. The "image reversal" by adjusting the pH provides a simple and effective approach for manipulating the amount and location of nanoscale building blocks assembled on plasma lithography patterned surface templates.

Introduction

Many nanoengineered structures and materials possess unique and novel characteristics compared to bulk materials.[1,2] For example, colloidal semiconductor nanocrystals, or quantum dots, display size-dependent photonic and electronic properties and are functional building blocks for engineering systems toward various applications, such as molecular diagnostics, biomolecular imaging, nanoelectronics, nanophotonics, and energy.[3–9] To realize the potential of quantum dots and other nanoscale materials, the ability to spatially arrange these materials is essential to engineer devices that combine top-down and bottom-up manufacturing strategies and have characteristic length scales spanning across several orders of magnitude. In particular, various microscale and nanoscale manufacturing approaches, such as photolithography, dip-pen nanolithography, electrokinetics, microcontact printing, and AFM-based manipulation, have been developed to guide the spatial arrangement of nanoengineered materials.[10–17] However, few existing techniques are capable of large-scale assembly of nanoscale building blocks with submicron scale resolution at low cost.

Recently, a plasma lithography technique that efficiently guides the assembly of quantum dots, biomimetic proteins and other nanoscale building blocks has been reported.[18–21] The technique has been applied in various chemical, biological, and engineering applications.[22,23] In this method, spatially selective plasma modification of polymer substrates is applied to create surface templates for guiding the assembly of nanoscale building blocks. The basic process of plasma lithography is shown in Fig. 1. A PDMS mold with micrometre or sub-micrometre scale structures is used to protect selective regions of a substrate from plasma surface modification while allowing plasma to treat other regions. This selective modification results in functionalized templates on the substrate replicating the design of the PDMS mold. After plasma modification, the substrates are incubated in a solution of nanoscale materials for self-assembly with the surface patterns providing a template to guide the self-assembly of the building blocks. After incubation, the substrate is removed from the solution and can be characterized by fluorescence microscopy or scanning electron microscopy. The use of plasma lithography provides several advantages when creating nanoscale structures. Firstly, resolution of the pattern of building blocks can be achieved from 100 nm to over 1 cm. Secondly, the batch processing nature of plasma lithography allows rapid nanomanufacturing compared to serial manufacturing techniques, such as laser machining, e-beam lithography and dip-pen nanolithography. Furthermore, plasma lithography is compatible to various substrate materials, such as glass, PDMS, and polystyrene, and is one of the few techniques that can be directly applied to polymeric materials taking advantages of the large selection of plasma gases. Polymeric materials are particularly useful for biomedical applications due to their biocompatibility. The technique is also applicable to pattern

[a]*Department of Aerospace and Mechanical Engineering, The University of Arizona, Tucson, AZ 85721, USA. E-mail: pak@email.arizona.edu*
[b]*Biomedical Engineering and Bio5 Institute, The University of Arizona, Tucson, AZ 85721, USA*

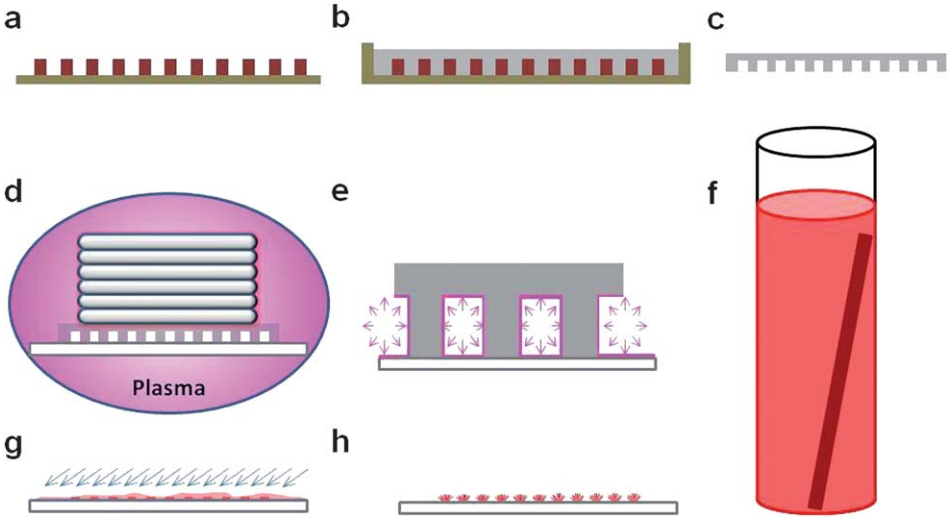

Fig. 1 Plasma lithography. (a) Photolithography or e-beam lithography defined master structures created out of photoresist. (b) PDMS was poured over master and cured. (c) and (d) The working mold is removed from master and placed on a polystyrene substrate. The weight was placed on the working mold to ensure conformal contact with the substrate. Substrate–mold–weight assembly was then plasma treated. (e) Selective plasma treatment functionalizes exposed areas. (f) The substrate was placed in the solution of quantum dots or other nanoscale building blocks for template-guided self-assembly. (g) and (h) The substrate was removed from the solution, then rinsed and dried revealing solute assembled onto the plasma lithography defined pattern.

various nanoscale building blocks for nanomanufacturing, including polystyrene nanoparticles, gold nanoparticles, salts, proteins, polyelectrolytes, and biomimetic proteins.[18–21]

Despite the advantages of plasma lithography, the governing mechanisms of the plasma lithography guided self-assembly technique are not well understood. In particular, relatively little is known about the factors that influence the deposition process including the pH of the solvent solution and the physicochemical characteristics of the nanoscale building blocks. Remarkably, gold nanoparticles, polystyrene spheres, and aluminium potassium sulfate salts are known to assemble on untreated, hydrophobic areas while quantum dots and human-α-thrombin assemble on plasma treated, hydrophilic areas.[19] The mechanisms that drive this selective deposition are not fully understood, and the possibility of controlling the assembly process by adjusting operating conditions has not been explored.

Among all the experimental conditions, the pH value is one of the most important factors that govern molecular and nanoscale self-assembly. For example, the pH of the solvent solution has been seen to affect self-assembly dramatically.[24,25] Another study has also found that a pH range exists to assemble charged quantum dots onto supported lipid bilayers.[26] In this study, the role of the pH value in the plasma lithography process was investigated. The results were characterized using fluorescence microscopy and scanning electron microscopy (SEM). In addition to colloidal quantum dots, the competitive binding of biological molecules, including bovine serum albumin (BSA), poly-L-lysine (PLL), and fluorescein isothiocyanate (FITC), was also tested under different pH values.

Materials and methods

Materials

Colloidal quantum dots used in this study were amino polyethylene glycol (PEG) modified quantum dots (Q21501MP) from Invitrogen (Carlsbad, CA) having an emission peak at 605 nm. The quantum dots were diluted in phosphate buffered saline (PBS) to achieve a 40 nM final concentration. Acetic acid, sodium bicarbonate and sodium hydroxide were added to the quantum dot solutions to adjust the pH. The pH was measured by a digital pH meter (Hanna Instruments). Sterile polystyrene Petri dishes (VWR, Inc) were used as substrates on which the quantum dots were assembled. FITC-conjugated BSA (A9771), FITC (F7250), and FITC-labeled PLL (P3069) were purchased from Sigma (St Louis, MO). For templates, optical gratings with 25 μm wide channels spaced 5 μm apart were utilized as master molds. Polydimethylsiloxane (PDMS; Dow Corning Corporation) used in this study was mixed at a curing agent to elastomer base ratio of 1 : 8. After thorough mixing, PDMS was degassed in a vacuum chamber for 5 min. Liquid PDMS was then poured onto the master mold to produce PDMS working molds. The PDMS molds were cured at 75 °C for 4 hours before use.

Plasma lithography

The plasma lithography process for template-guided self-assembly is shown in Fig. 1. Briefly, working PDMS molds were cut into ~1 cm by 1 cm squares (Fig. 1a–c) and placed on a polystyrene substrate with a weight that generates ~5 to 10 kPa of pressure to ensure conformal contact between the working mold and the polystyrene substrate (Fig. 1d and e). The substrate was then exposed to air plasma treatment at a radio frequency power of 30 W at 150 Pa for 10 minutes in a plasma cleaner (PDC-001, Harrick Plasma). After plasma treatment, the plasma treated regions of the substrate are modified to be hydrophilic and have a contact angle of ~10° compared to fresh polystyrene which has a contact angle of ~81°. This is achieved by introducing oxygen-based functional groups as determined by X-ray photoelectron spectroscopy.[19] Due to physical shielding of the PDMS mold, a spatial plasma-functionalized surface pattern was

generated. After plasma treatment, PDMS molds were removed and the substrate was immediately immersed into the building block solutions (Fig. 1f). The templates of surface chemistry created by the plasma can be preserved for long-time periods (over 2 months) in buffer solutions. In the current study, the samples were incubated in solution for 24 hours and the assembly process could reach equilibrium in ~10 hours (data not shown). The samples were then taken out and rinsed three times with deionized water before imaging (Fig. 1g and h).

Imaging

The samples were observed using an inverted epi-fluorescence microscope (Leica Microsystems, Wetzlar, Germany), and fluorescence images were captured by a CCD camera (SensiCam, PCO, Kelheim, Germany). The amino PEG modified quantum dots were illuminated by a mercury lamp with a band-pass excitation filter of 515–560 nm. Images were recorded with a 580 nm dichromatic mirror and a long-pass filter of 590 nm. The FITC and its labeled materials were illustrated using a band-pass filter of 450–490 nm; the images were recorded with a 510 nm dichromatic mirror and a long-pass filter of 515 nm. The background fluorescence of each polystyrene substrate was subtracted from images for image analysis. Scanning electronic microscope (SEM) images were obtained using a field-emission SEM (Hitachi S-4800 Type II, Tokyo, Japan). All images were analyzed using ImageJ software (National Institutes of Health, USA).

Results and discussion

Amino (PEG) functionalized quantum dots were first tested for assembling on polystyrene substrates patterned by plasma lithography. The mold used has alternative line patterns of open regions (*i.e.*, plasma treated) 25 μm in width and shielded regions (*i.e.*, untreated) 5 μm in width. Fig. 2 shows the fluorescence images of quantum dots self-assembled on the pattern under different pH values. The pH of the solvent has a strong influence on the area to which the quantum dots assemble. The quantum dots preferentially assemble on treated or untreated areas depending on the pH. At pH below 9, the majority of quantum dots are assembled on the hydrophilic, plasma-treated region of the substrate. At pH above 9, the quantum dots prefer to assemble on the hydrophobic, native polystyrene area. This provides a simple and effective approach for creating "image reversal" such that the nanoscale building blocks can be deposited differently on the same pattern.

To investigate the results quantitatively, the fluorescence intensities in the treated and untreated areas of the substrate were measured as a function of the pH of the solvent solution (Fig. 3). A large (2 mm) circular pattern was used for measuring the intensity of the florescence to avoid fluorescence blooming. Examination of intensities reveals that the fluorescence intensity on the treated area, which indicates the amount of quantum dots deposited, is relatively constant in weak acidic solvent solutions (between pH 4.41 and 6.23). With increasing pH above 7, however, the intensity on the treated area decreases significantly. On the other hand, the intensity on the untreated area decreases only slightly in the entire range tested (4.41 to 10.83). With the rapid decrease of intensity in the treated area, the contrast value (*i.e.*, the difference in intensities between treated and untreated areas) switches from positive to negative at approximately pH 9. At this transition pH, the favorable region for quantum dot assembly changes from the treated to the untreated region.

In addition to fluorescence microscopy, SEM was performed to examine the quantum dots assembled on the substrate and to quantify the amount of quantum dots in the treated and untreated regions. As shown in Fig. 4, the quantum dots assemble into a dense layer on the substrate and the density

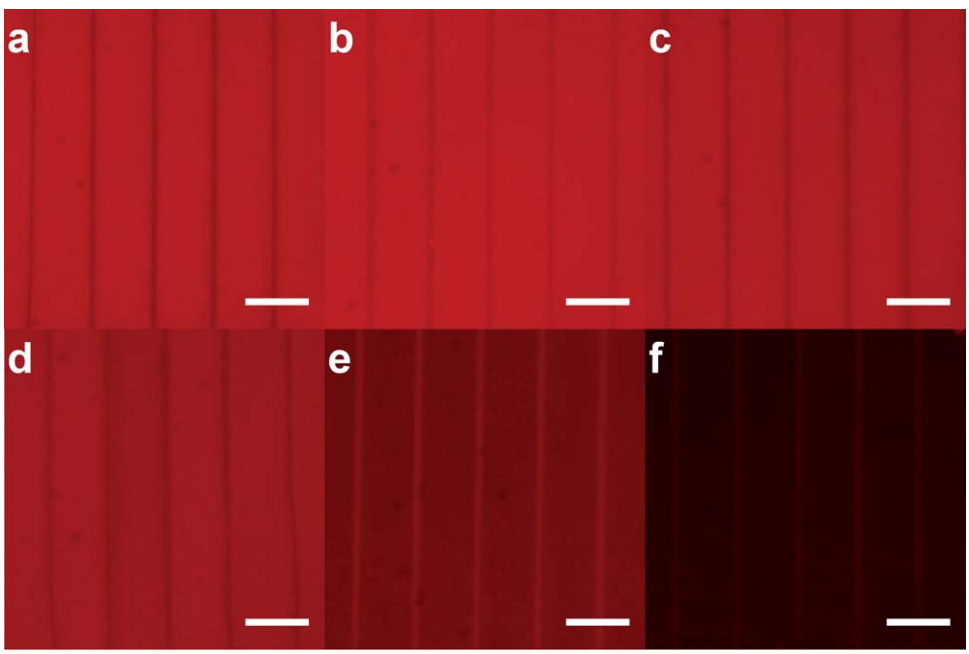

Fig. 2 Quantum-dots assembly using plasma lithography at different pH. The pH of solutions from (a) to (g) are 5.05, 7.12, 7.81, 8.71, 9.28, and 9.51, respectively. Scale bars are 25 μm.

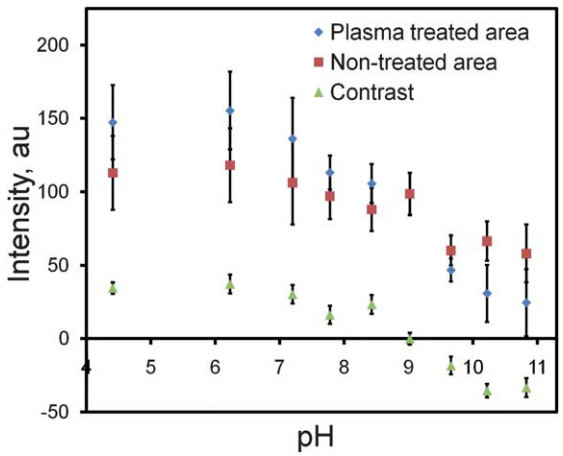

Fig. 3 Comparative binding of amino-functionalized quantum dots at different pH values characterized by fluorescence intensity. Data represent mean ± standard deviation.

depends on the pH and the area to which the quantum dots assemble. To estimate the density, the number of quantum dots deposited on the plasma-treated region and native polystyrene surface was counted. In general, the SEM observation is consistent with the fluorescence characterization. The quantum dot density decreases with the pH on the treated area, while the density of quantum dots assembled on the untreated areas is relatively constant. The transition of the favorable region for quantum dots assembly occurred at approximately pH 9, which is consistent with the fluorescence measurement.

The comparative binding process can be understood by considering the major interactions between the substrate and quantum dots, namely electrostatic and van der Waals interactions. The electrostatic force strongly depends on the surface functional groups. The substrate possesses different amounts of interfacial charge depending on the pH of the solvent solution and can be characterized by the point of zero charge (PZC) and pK_a. PZC is the pH value such that the electrical charge density on a surface is zero. A surface is positively charged below the PZC and is negatively charged above the PZC. For polystyrene treated with air plasma, oxygen-based functional groups are introduced onto the surface and the PZC of the plasma-treated polystyrene surface has been determined to be 2.5.[27] Therefore, the plasma-treated surface is always negatively charged in our experimental condition (pH above 4.41). As the pH increases, the ζ potential increases and the net negative charge on the substrate increases. The charge typically reaches a plateau at a high pH. In the same manner, the charges on the quantum dots are also affected by the pH of the solvent. Due to protonation in an acidic solvent, the amino-functionalized quantum dots are positively charged at low pH. When the pH is smaller than the pK_a, the majority of amino groups are protonated, and thus positively charged. This facilitates the deposition of positively charged quantum dots onto the negatively charged substrate through electrostatic interactions. This is consistent with our observation that the quantum dots preferentially bind to the treated surface in weak acidic solution (between pH 4.41 to 6.23).

With an increase in pH, the charge on the plasma-treated area remains negative and the positive charge of the quantum dots

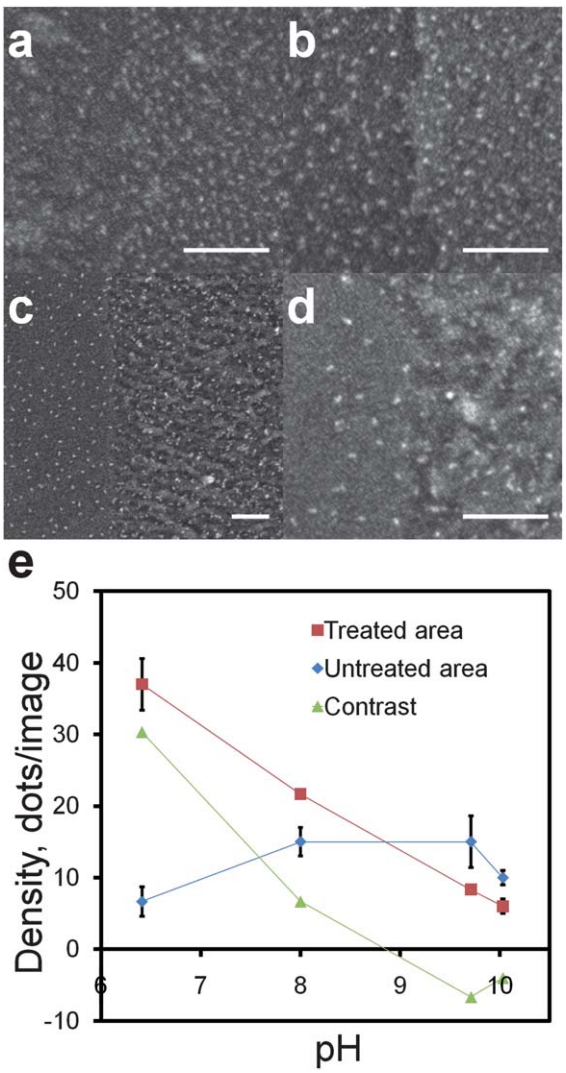

Fig. 4 SEM characterization of quantum dots self-assembled at the hydrophobic–hydrophilic interface. (a–d) The pH of quantum dot solutions are (a) 6.75, (b) 8.0, (c) 9.41, and (d) 10.03. (e) The quantum dot density as a function of the pH of the buffer solutions. Data represent mean ± standard deviation.

should reduce significantly at pH values near the pK_a. In our experiment, the pK_a of amino-functionalized quantum dots is between 9 and 10[26] and is in agreement with the significant decrease in the number of quantum dots on the treated area observed at pH from 7 to 10. This suggests the involvement of electrostatic interactions in the binding process of amino-functionalized quantum dots. At pH $\gg$ pK_a, the amino groups are fully deprotonated and the electrostatic interaction diminishes. In this situation, the van der Waals interaction is likely to play a more important role. This hypothesis is supported by the fact that the quantum dots are assembled onto the untreated, hydrophobic area in the entire range tested independent of the pH. Furthermore, the amounts of quantum dots assembled on the treated and untreated areas also correlate with the surface roughness. At the nanoscale, a rough surface can increase the effective distance between the surface and the object. Since the van der Waals interaction strongly depends on the distance, it is

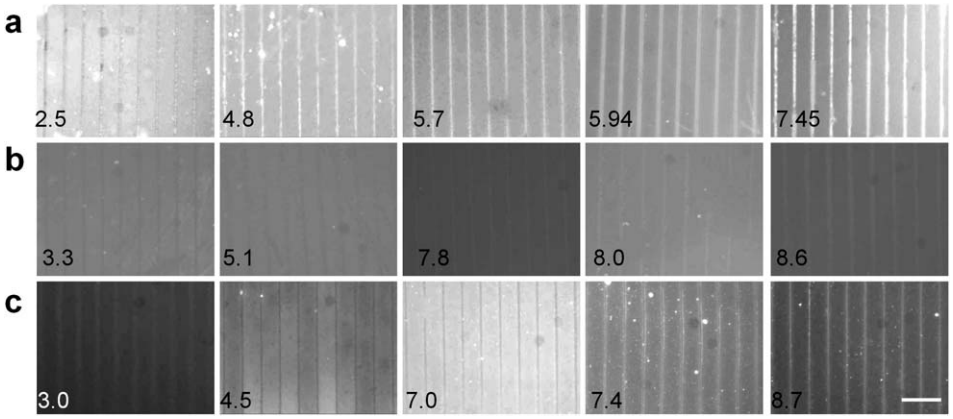

Fig. 5 Comparative bindings of nanoscale building blocks: (a) BSA, (b) FITC, and (c) PLL. The pH values of the buffer solution are marked on the images. The scale bar represented is 50 μm.

anticipated to decrease with the surface roughness.[28] The plasma treatment is known to increase the roughness of the polystyrene surface from 1.2 ± 0.2 nm to 3.8 ± 0.7 nm, as characterized by atomic force microscopy.[19] Thus, the van der Waals force of the untreated surface is anticipated to be greater than that of the treated region. In our experiments, a larger amount of quantum dots is attached on the untreated area compared with the treated area in high pH (above pH 9) solutions. This supports that the van der Waals interaction is involved in the competitive assembly process and dominates over electrostatic force in high pH values. These results support the hypothesis that the switching between the dominance of electrostatic and van der Waals interactions is a major reason for the observed "image reversal" of the assembly process.

In addition to amino (PEG) quantum dots, other building blocks were evaluated to investigate the comparative binding process (Fig. 5). Fig. 5a shows the assembly of FITC-labeled BSA from pH 2.5 to 7.45. Similar to quantum dots, the assembly of BSA displays a strong pH dependency. BSA generally adheres to the treated area at low pH and to the untreated area at high pH. In the experiment, the transition pH value for BSA occurred between 2.5 and 4.8. This is in good agreement with the fact that the isoelectric point of BSA is approximately 4.6,[29,30] and suggests that BSA may follow similar comparative binding mechanisms as in quantum dots. Since BSA was labeled with FITC for facilitating fluorescence observation, the assembly of FITC alone was also tested as a control. As shown in Fig. 5b, FITC only bound weakly to the surface, as indicated by the low intensity. Despite the weak binding between FITC and the substrate, strong pH dependence for FITC assembly and image reversal can also be observed. The transition pH occurs between pH 5.1 and 7.8. These results further support that the plasma lithography assembly process can be understood by the competition between electrostatic and van der Waals interactions.

The pH dependence of PLL assembly on plasma patterned templates was also investigated. Remarkably, two transition pH values were observed for PLL. The first transition pH is between 3.0 and 4.5 and the preferred area for molecular binding switches from the untreated to the treated areas. The second transition point occurs between 7.0 and 7.4 and the preferred binding area changes from treated to untreated areas. The reason for the addition transition at low pH is not clear and may be explained by the difference in the electrostatic and van der Waals interactions for PLL assembly. Since PLL is highly charged and has a relatively high isoelectric point,[31] the relative importance of each force for PLL could be different from BSA and quantum dots. The difference could also be a result of the intermolecular electrostatic interactions between the PLL molecules and the molecular configuration of the long chain polymer. Further investigation is required to elucidate these observations. Nevertheless, PLL and other molecules can be effectively assembled on plasma lithography patterned templates and their assembly can be manipulated by properly adjusting the pH.

Conclusion

In this study, the comparative binding of several nanoscale building blocks on plasma lithography patterned substrates at equilibrium was examined. Adjustment of the buffer pH is shown to be a simple and effective way for controlling the template-guided self-assembly process. In addition to electrostatic forces, van der Waals interactions play an essential role in the assembly process. Future investigations are focusing on the binding mechanisms for different nanoscale building blocks and the kinetics of the binding process in different regions. The simplicity and effectiveness of plasma lithography is anticipated to allow plasma lithography to be used for a wide spectrum of engineering and biological applications such as quantum dot wave guides and geometric control of neuronal differentiation.[22,32–35]

Acknowledgements

We thank Dr Brook Beam from the University of Arizona's Keck Facility for assistance in SEM imaging. This work is supported by the NIH Director's New Innovator Award (1DP2OD007161-01) and NSF Nanomanufacturing (0855890).

References

1 M. C. Roco, *Sci. Am.*, 2006, **295**, 39.
2 P. K. Wong and D. Ho, *IEEE Nanotechnology Magazine*, 2008, **2**, 9–13.
3 A. P. Alivisatos, *Science*, 1996, **271**, 933–937.
4 M. Y. Han, X. H. Gao, J. Z. Su and S. Nie, *Nat. Biotechnol.*, 2001, **19**, 631–635.

5 C. Y. Zhang, H. C. Yeh, M. T. Kuroki and T. H. Wang, *Nat. Mater.*, 2005, **4**, 826–831.
6 T. H. Wang and P. K. Wong, *J. Assoc. Lab. Autom.*, 2010, **15**, A15–A16.
7 Y. Lei, S. K. Yang, M. H. Wu and G. Wilde, *Chem. Soc. Rev.*, 2011, **40**, 1247–1258.
8 Y. Li, N. Koshizaki and W. P. Cai, *Coord. Chem. Rev.*, 2011, **255**, 357–373.
9 N. Koshizaki, Y. Li, T. Sasaki and Y. Shimizu, *J. Am. Chem. Soc.*, 2008, **130**, 14755–14762.
10 A. Perl, D. N. Reinhoudt and J. Huskens, *Adv. Mater.*, 2009, **21**, 2257–2268.
11 R. D. Piner, J. Zhu, F. Xu, S. Hong and C. A. Mirkin, *Science*, 1999, **283**, 661–663.
12 R. H. M. Chan, C. K. M. Fung and W. J. Li, *Nanotechnology*, 2004, **15**, S672–S677.
13 M. L. Y. Sin, V. Gau, J. C. Liao, D. A. Haake and P. K. Wong, *J. Phys. Chem. C*, 2009, **113**, 6561–6565.
14 T. Junno, K. Deppert, L. Montelius and L. Samuelson, *Appl. Phys. Lett.*, 1995, **66**, 3627–3629.
15 D. H. Kim, P. K. Wong, J. Park, A. Levchenko and Y. Sun, *Annu. Rev. Biomed. Eng.*, 2009, **11**, 203–233.
16 L. Guangyong, X. Ning, Y. Mengmeng and F. Wai-Keung, *IEEE ASME Trans. Mechatron.*, 2004, **9**, 358–365.
17 D. Graham, A. Hernandez-Santana, E. Irvine and K. Faulds, *Chem. Sci.*, 2011, **2**, 211–215.
18 J. Keyes, M. Junkin, J. Cappello, X. Wu and P. K. Wong, *Appl. Phys. Lett.*, 2008, **93**, 023120.
19 M. Junkin, J. Watson, J. P. V. Geest and P. K. Wong, *Adv. Mater.*, 2009, **21**, 1247–1251.
20 B. A. Langowski and K. E. Uhrich, *Langmuir*, 2005, **21**, 10509–10514.
21 A. Khademhosseini, K. Y. Suh, S. Jon, G. Eng, J. Yeh, G.-J. Chen and R. Langer, *Anal. Chem.*, 2004, **76**, 3675–3681.
22 M. Junkin, S. L. Leung, Y. Yang, Y. Lu, J. Volmering and P. K. Wong, *J. Vis. Exp.*, 2011, **52**, DOI: 10.3791/3115.
23 M. Junkin and P. K. Wong, *Biomaterials*, 2011, **32**, 1848–1855.
24 T. Zhu, X. Fu, T. Mu, J. Wang and Z. Liu, *Langmuir*, 1999, **15**, 5197–5199.
25 N. Kameta, H. Minamikawa, M. Masuda, G. Mizuno and T. Shimizu, *Soft Matter*, 2008, **4**, 1681–1687.
26 X. Zhang and S. Yang, *Langmuir*, 2011, **27**, 2528–2535.
27 C. C. Dupont-Gillain, Y. Adriaensen, S. Derclaye and P. G. Rouxhet, *Langmuir*, 2000, **16**, 8194–8200.
28 M. Savia and Z. Quan, *IEEE/RSJ International Conference on Intelligent Robots and Systems (IROS)*, 2010.
29 S. Bingaman, V. H. Huxley and R. E. Rumbaut, *Microcirculation*, 2003, **10**, 221–231.
30 S. H. Brewer, W. R. Glomm, M. C. Johnson, M. K. Knag and S. Franzen, *Langmuir*, 2005, **21**, 9303–9307.
31 D. Wang and L. Chen, *Nano Lett.*, 2007, **7**, 1480–1484.
32 L. D. Huang, C. J. Wang and L. Y. Lin, *Opt. Lett.*, 2007, **32**, 235–237.
33 M. Hegg and L. Y. Lin, *Opt. Express*, 2007, **15**, 17163–17170.
34 M. Song and K. E. Uhrich, *Ann. Biomed. Eng.*, 2007, **35**, 1812–1820.
35 L. D. Huang, C. C. Tu and L. Y. Lin, *Appl. Phys. Lett.*, 2011, **98**, 113110.